ORIGINAL RESEARCH ARTICLE

Three-Stage Method Energy–Mass Coupling High-Efficiency Utilization Process of High-Temperature Molten Steel Slag

WEIBIN CHEN, MINGHAO WANG, LILI LIU, HAO WANG, and XIDONG WANG

High-temperature molten steel slag is a large amount of industrial solid waste containing available heat energy and resources. This paper introduces an efficient and comprehensive utilization process of high-temperature molten steel slag. The waste heat energy in the high-temperature molten steel slag can be fully recovered through the three-stage heat exchange. Through mass balance and energy balance, the theoretical heat recovery rate can reach 81.42 pct when the waste heat stored in steel slag is converted into usable heat energy, and the exergy efficiency of the overall system is 27.93 pct. When the waste heat stored in the steel slag is converted for electric energy, the theoretical heat recovery rate can reach 24.49 pct, and the exergy efficiency of the overall system is 33.83 pct. When the waste heat stored in steel slag is used for cogeneration, the theoretical heat recovery rate can reach 83.98 pct, and the exergy efficiency of the overall system is 38 pct. The normal-temperature solid steel slag produced by the process is easy for iron selection and subsequent high value-added utilization. The solidification of steel slag in this process consumes a large amount of CO_2 so that the free calcium oxide (f-CaO) in the steel slag is fixed, which is more conducive to subsequent utilization, thereby achieving the purpose of energy saving and emission reduction. Compared with the utilization of traditional steel slag, this process can better utilize the energy and resources contained in steel slag and provides a new method for fully utilizing the waste heat energy and resource attributes of high-temperature molten steel slag.

https://doi.org/10.1007/s11663-021-02213-7

I. INTRODUCTION

ENERGY is the cornerstone of the development of human society and the most basic element for developing social economy and civilization. The steel industry consumes 9 pct of the total energy consumption [1], and it currently accounts for about 7 pct of energy sector CO_2 emissions (including process emissions).[2] In October last year, the International Energy Agency (IEA) released its *Iron and Steel Technology Roadmap*.[2] This document presented a vision and advanced measures for the steel industry in line with the *Paris Agreement*. According to the IEA's Sustainable Development Scenario, compared with 2019, direct emissions from the iron and steel sector should be reduced by more than 50 pct by 2050. It is a great challenge for the iron and steel sector to meet this demand as it tries to chart a more sustainable path while remaining competitive. Figure 1(a) shows the crude steel production in China and the world in the last decades.[3] The steel production of the whole world, especially in China, has been rising in this period. Global crude steel production reached 1864.0 million tonnes (Mt) in 2020. The COVID-19 crisis has posed serious challenge to global supply chains, resulting in an estimated 0.9 pct decline in global crude steel production in 2020 compared with 2019. The People's Republic of China adapts to the global trend, with its output increased in 2020. China's crude steel production reached 1053.0 Mt in 2020, up by 5.2 pct on 2019. China's share of global crude steel production increased to 56.5 pct in 2020 from 53.3 pct in 2019. Therefore, the energy conservation of China's steel industry has great significance for the world. The steel industry still has enormous energy-saving potential, among which the available heat energy of high-temperature slag occupies an important position.[4] High-temperature molten slag, mainly including blast furnace slag and steel slag, is produced in the iron-making and steel-making process, and its temperature is about 1673

WEIBIN CHEN, MINGHAO WANG, LILI LIU, HAO WANG, and XIDONG WANG are with the Department of Energy and Resources Engineering, College of Engineering, Peking University, 100871 Beijing, PR China and also with the Beijing Key Laboratory for Solid Waste Utilization and Management, Peking University, 100871 Beijing, PR China. Contact e-mail: pkuwanghao@pku.edu.cn; xidong@pku.edu.cn.

Manuscript received November 19, 2020; accepted May 4, 2021.
Article published online June 14, 2021.

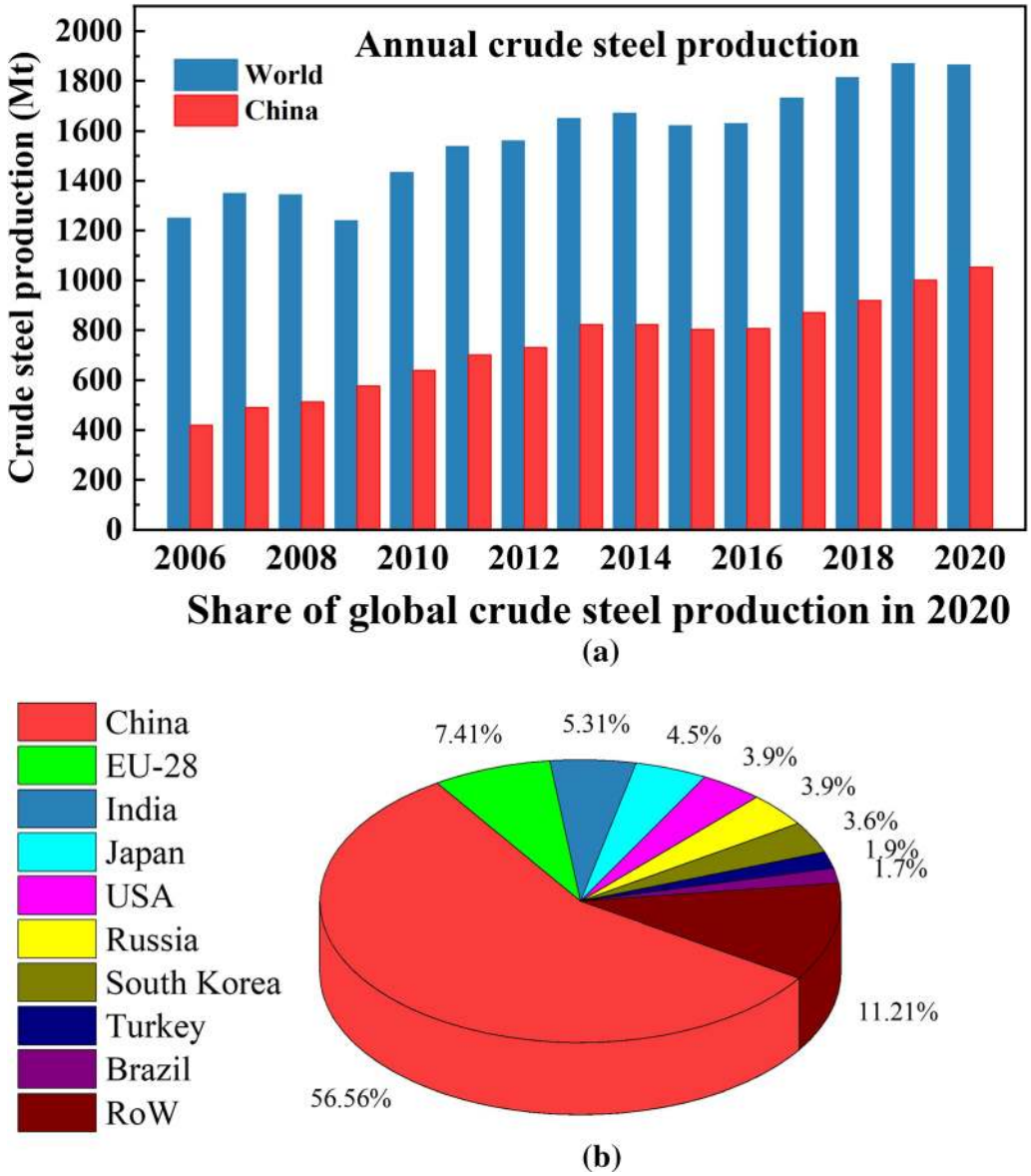

Fig. 1—(*a*) Annual crude steel production in recent years. (*b*) Share of global crude steel production in 2020.

to 2023 K.[5] The typical chemical composition of steel slag is shown in Table I.[6] Steel slag is made up of silicates, alumina silicates, calcium aluminum silicates, and iron oxides.[7] During the steel-making process, a proportion of the molten iron cannot be recovered so elemental iron is often observed in the slag. Therefore, compared with blast furnace slag, steel slag generally contains more ferrous phases.[8] In slag characterization, basicity refers to the ratio of CaO to SiO_2 in a slag sample.[9] Steel slag has higher basicity,[10] so its utilization is also very different from blast furnace slag.[11] In particular, rapid crystallization leads to a rapid increase in the viscosity of steel slag, so its crushing and granulation are more difficult. Therefore, the utilization rate of steel slag is much lower than that of blast furnace slag. The slag often contains a large amount of harmful and heavy metals, so the uses of slag have to be carefully managed to ensure no environmental impact.[12]

Scholars have been exploring the recycling of steel slag since the 1970s, mainly focusing on returning steel slag to the blast furnace as a solvent. In the 1980s, scholars began to explore the application of steel slag in the construction industry.[13] It has been found that steel slag can be broadly applied in the construction field, for example, to be used in blended cement manufacturing[14,15]; to be used as a granular material in road base or subbase courses[16,17] or an aggregate in various asphalt mixes or pavement surfaces.[18–20] In particular, making cement from steel slag has received widespread attention,[21–23] but the *free lime volume instability* of steel slag limits this application.[24] This is mainly because steel slag contains the f-CaO mineral phase,[25,26] f-CaO hydrates to form $Ca(OH)_2$ when it meets water,[27] which causes cracking of concrete engineering, roads, and building materials. For example, if the steel slag is used in a road surface that gets wet, the free lime expansion can cause the road surface to

fracture.[28] Steel slag volume expansion has been recorded to be as much as 10 pct.[29] Therefore, before steel slag is prepared for building materials, measures need to be taken to remove f-CaO.[30,31] In recent years, China's research on the utilization of steel slag has mainly focused on the treatment of steel slag by the thermal braising method.[32–34] The thermal braising method is to heat the steel slag under the conditions of steam and high pressure. Through the thermal braising treatment, the unstable mineral phase contained in it is converted into stable minerals. However, this method does not make full use of the steel slag's waste heat, which limits its further development. So far, scholars around the world have researched and developed nearly 50 methods for the comprehensive utilization of steel slag.[25,35–38] However, there is no effective way for the large-scale resource utilization of steel slag, which is a worldwide issue.

This paper proposes a waste heat recovery and resource utilization technology for molten steel slag, which can effectively improve the heat recovery efficiency. After the waste heat utilization, the steel slag improves its stability and can be used as a raw material for building materials. The molten steel slag is fully cooled through three-stage heat exchange, and the heat in it is fully recovered. This paper introduces the basic principles of the process route and the equipment. The heat recovery efficiency and exergy efficiency are also calculated through mass balance and energy balance.

II. TECHNOLOGICAL PROCESS AND EQUIPMENT DESIGN

A. *Technological Process*

As shown in Figure 2, high-speed air is used as the heat recovery medium to rapidly cool the high-temperature molten steel slag in the first stage of heat recovery, accompanied by the centrifugal granulation of steel slag. The steel slag is granulated by centrifugation to form steel slag droplets, comprising high-temperature solid steel slag. In the second stage, cooling water serves as the heat recovery medium. The high-temperature solid steel slag is cooled by the waterwall down to medium temperature. In the third stage, CO_2 is the heat recovery medium. Through counterflow heat exchange, the normal-temperature CO_2 and the medium-temperature solid steel slag change into normal-temperature solid steel slag and high-temperature CO_2. Moreover, at this stage, the f-CaO in the steel slag can generate $CaCO_3$ with CO_2 so that f-CaO was resolved quickly, which simultaneously promotes the quick recovery and immediate stabilization of steel slag. The heat contained in the high-temperature air, high-temperature water vapor, and high-temperature CO_2 obtained in the process can be further recovered, and the waste heat can be converted into heat energy or electric energy, which will be analyzed in-depth in the following discussion.

B. *Equipment Design*

The equipment for the three-stage energy–mass coupling of molten steel slag is shown in Figure 3. First, the high-temperature molten steel slag transported by the slag tanker enters the molten slag buffer system. A stopper controls the flow rate of the slag entering the granulation system. Subsequently, the molten steel slag enters the granulation system through the molten slag buffer and drainage system. Under the action of friction and centrifugal force, the molten steel slag is thinned, filmed, broken on the high-speed rotating granulation disk, and shrinks into slag droplets because of surface tension. The physical model of high-temperature molten steel slag film breaking is shown in Supplementary Figure S1**. (**Refer to electronic supplementary material*). The slag particles leaving the disk are finely divided into smaller ones. The slag particles cool and solidify

Table I. Constituents of Steel Slag, Mass Percent

CaO	SiO_2	FeO	Al_2O_3	MgO	MnO	TiO_2	Cr	P	S
30 to 35	8 to 20	10 to 35	1 to 6	5 to 15	2 to 8	0.4 to 2	0.1 to 0.5	0.2 to 2	0.05 to 0.15

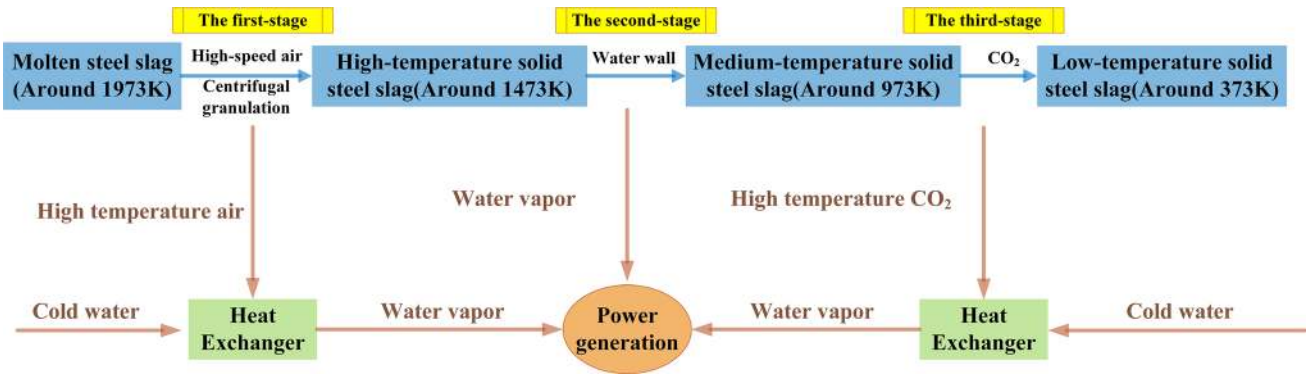

Fig. 2—Technical roadmap for efficient utilization of three-stage high-temperature molten steel slag.

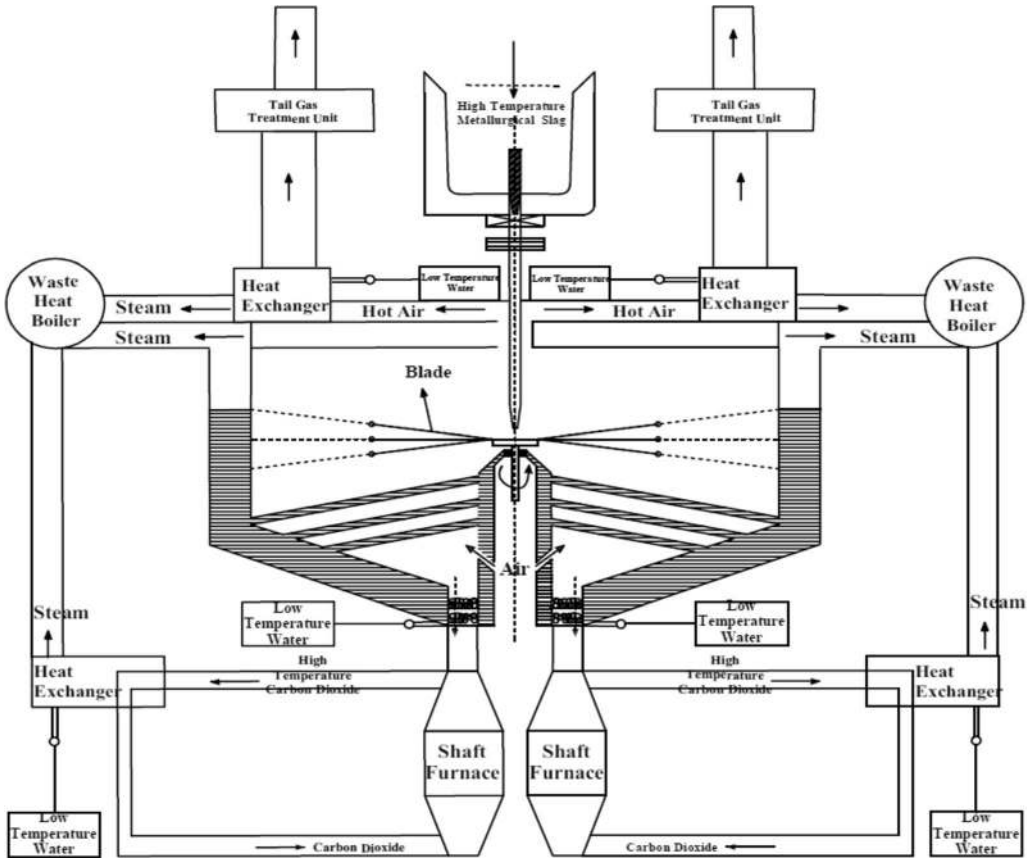

Fig. 3—Schematic diagram of equipment for energy–mass coupling of molten steel slag.

during flight. The physical model of high-temperature molten steel slag and the schematic diagram of the solidification process are shown in Supplementary Figure S2. We also conducted a simulation of the heat exchange process at this stage using the commercial computational fluid dynamics (CFD) package software *ANSYS Fluent* (Supplementary Figure S3). In this process, a large amount of sensible heat of the slag exchanges heat with the air. In order to ensure the heat exchange efficiency between air and steel slag, fresh air is continuously introduced, and high-temperature air is discharged to ensure that the temperature of the air is low enough. The granulation chamber's shell is made in waterwall structure, within there are also water-cooling layers. The waterwall is made of two layers of 2 to 5 mm metal, between which can be filled with circulating water. The steel slag particles hit the cooling wall to fully exchange heat, and gradually slide down to the bottom. Next, they are discharged into the shaft furnace through the slag discharge system. Then, the granulated slag particles and CO_2 move countercurrently to exchange heat in the shaft furnace. Finally, the high-temperature air produced by the first stage of the heat exchange system is used to heat the cool water, and the water turns into high-temperature steam. In the second stage, Water's heat exchange in the waterwall also produces high-temperature steam. The high-temperature CO_2 produced by the third stage is converted into normal-temperature CO_2 after heat exchange with water. The normal-temperature CO_2 can be reused, and the heat produced by water is converted into water vapor. The steam produced during the whole process can enter the heat recovery steam generator (HRSG) for power generation and thermal energy utilization.

III. RESULTS AND DISCUSSION

A. *Thermodynamic Analysis*

In the first stage of heat exchange, the air has a strong oxidation effect on high-temperature steel slag. The FeO phase in the steel slag is oxidized, the unstable phase of lime-containing FeO is reduced, and the stable phase of $2CaO{\cdot}Fe_2O_3$ increases. In the third stage, the steel slag contains a large amount of unstable CaO, which reacts with CO_2 to form stable calcium carbonate.

As shown in Figure 4, the thermodynamic analysis is under the guidance of Gibbs free energy. The first stage of heat exchange is mainly about the oxidation of the iron-containing phase in steel slag. The iron-containing phases in steel slag can be divided into four types: Fe, FeO, Fe_3O_4, and Fe_2O_3. As shown in Figure 4, Eqs. [1–3] represent the reaction between the iron-containing phase and oxygen. When the temperature is below 1700 K, each reaction standard's Gibbs free energy is less than 0. Therefore, the iron-containing phase will spontaneously change from a low-valence

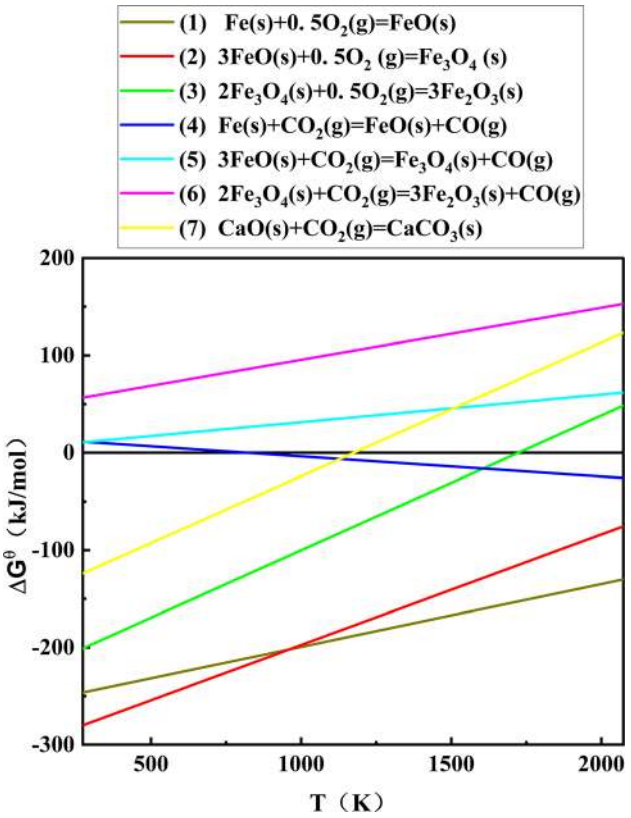

Fig. 4—Change of Gibbs free energy in related reactions.

state to a high-valence state. However, in this process, the heat exchange happens within a very short reaction time, which results in a low phase conversion rate, and the iron in the steel slag still maintains a low-valence state. Equations [4–6] represent the reaction of the iron-containing phase with CO_2. It can be seen that the iron will not be oxidized by CO_2 when the temperature is below 821.2 K. When the temperature is lower than 1063.1 K, Fe will be oxidized by CO_2 forming FeO. Fe_3O_4 in CO_2 atmosphere will not be oxidized at any temperature. Therefore, compared with air, using CO_2 to exchange heat is more conducive to reducing oxidation of the iron-containing phase and improving its recovery in the third stage.

The reaction of f-CaO in steel slag with CO_2 is very important. In response to the urgent need for the steel industry's CO_2 emission reduction, CO_2 mineralization has been considered one of the imperative strategies.[39,40] The use of steel slag for CO_2 mineralization is an interesting research area. Many scholars have done relevant research on the absorption of CO_2 by steel slag. Huijgen *et al.*[41] studied the carbonation reaction mechanism of using steel slag as a raw material to fix CO_2. They found that the particle size and reaction temperature are the most important factor influencing the rate of carbonation reaction. Under the operating conditions that the particle size is less than 38 μm, the reaction temperature is 373.15 K, the CO_2 partial pressure is 19 bar, and the reaction time is 30 minutes, the steel slag can reach the maximum carbonization rate of 74 pct. Bonenfant *et al.*[42] studied the fixation effect of steel slag on CO_2 under normal temperature and pressure. The results show that the CO_2 fixation capacity of steel slag can reach 247 gCO_2kg^{-1}. The content of free calcium hydroxide in steel slag is a key factor that determines the ability of CO_2 fixation. Chang *et al.* [43,44] showed that converter steel slag has a better CO_2 fixation effect than other types of steel slag, and its carbonation rate can reach 72 pct under the optimal reaction conditions. They also pointed out that reaction temperature and reaction time are the two most important factors affecting the carbonation effect of steel slag solution to fix CO_2, and used shrinking-core model and surface coverage model to explain the reaction kinetics mechanism of carbonation between steel slag and CO_2. Pan and Chiang[45] found that the flue gas CO_2 was rapidly mineralized into calcite precipitates using steel slag, and the maximum carbonation conversion of 86.3 pct, corresponding to a capacity of 0.38 t-CO_2 per ton of slag, can be obtained at 55 °C. Yu and Wang[46] carried out the research about how steel slag fixes CO_2. Studies have shown that, in general, the higher the temperature is, the higher the conversion rate of CaO in steel slag is. Ghouleh *et al.* made a compacted steel slag testing block, and its absorption ratio of CO_2 is 13 pct.[47] Shen *et al.*[48] found that the 2.5 pct phosphogypsum can promote the carbonization effect of steel slag, and under both paste and pressure conditions, the carbonization ratio of the slag is 52.1 pct. Wu and Dong's experimental research on the carbonation reaction of CaO powder or steel slag also showed that the temperature range of the rapid carbonation reaction of CaO is 723 to 1123 K, and the reaction speed is the fastest at about 973 K. This is consistent with the expected temperature of the steel slag in the third stage of this paper. Therefore, combined with the results of the experimental study, the reaction of steel slag and CO_2 is feasible both in thermodynamics and kinetics.

In the first stage, f-CaO doesn't react with oxygen and nitrogen in the air. When the cooling atmosphere of the third stage is CO_2, f-CaO can form $CaCO_3$ with CO_2. It can be seen from Figure 4 that as long as the temperature is below 1175.4 K, the reaction equation [7] proceeds spontaneously, and the unstable f-CaO is converted into stable $CaCO_3$. Through thermodynamic analysis, this technical route helps reduce oxidation of the iron-containing phase, while promoting the conversion of f-CaO. It is beneficial to the iron recovery of steel slag, the stabilization of the f-CaO phase, and the comprehensive utilization of tailings. We conducted an experiment of the reaction between steel slag and CO_2 in a fixed bed reactor in the laboratory (Supplementary Figure S5), in which the temperature was 973 K, and the pressure was normal pressure. The composition of the steel slag before and after the reaction is analyzed (Supplementary Figure S6). It can be seen that the f-CaO content in the steel slag is 6.8 pct. The f-CaO content only changes slightly with air atmosphere. When the slag reacts with CO_2 gas, the f-CaO content in the steel slag has been less than 2 pct. This also shows that using CO_2 to fix f-CaO in steel slag is effective. Therefore, it can be calculated from this experimental

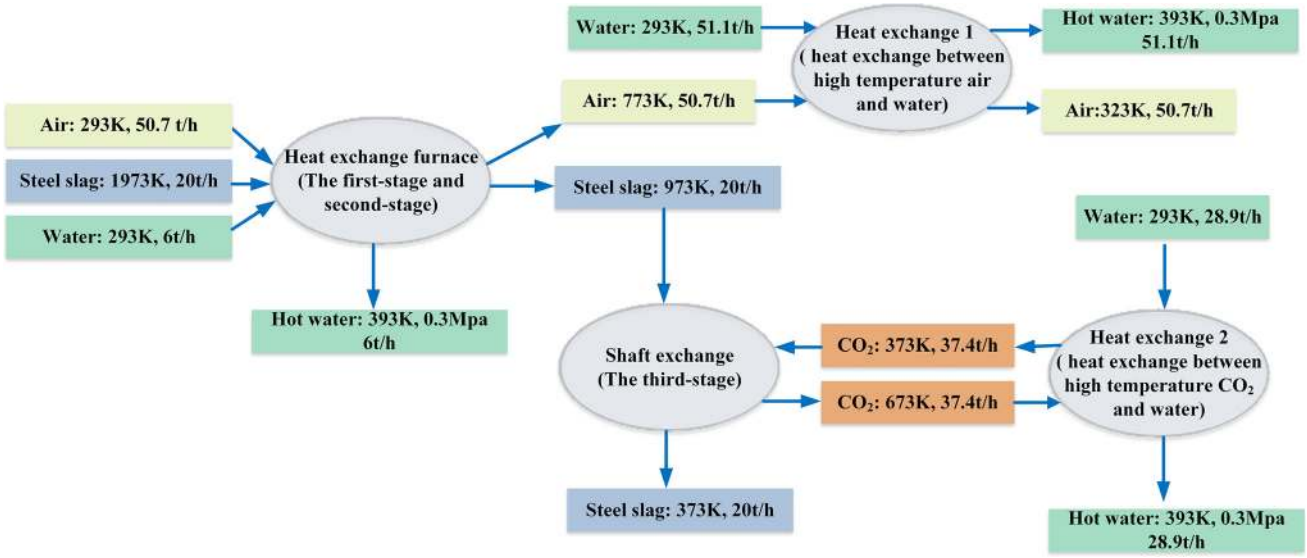

Fig. 5—The mass balance diagram of waste heat converted into usable heat energy.

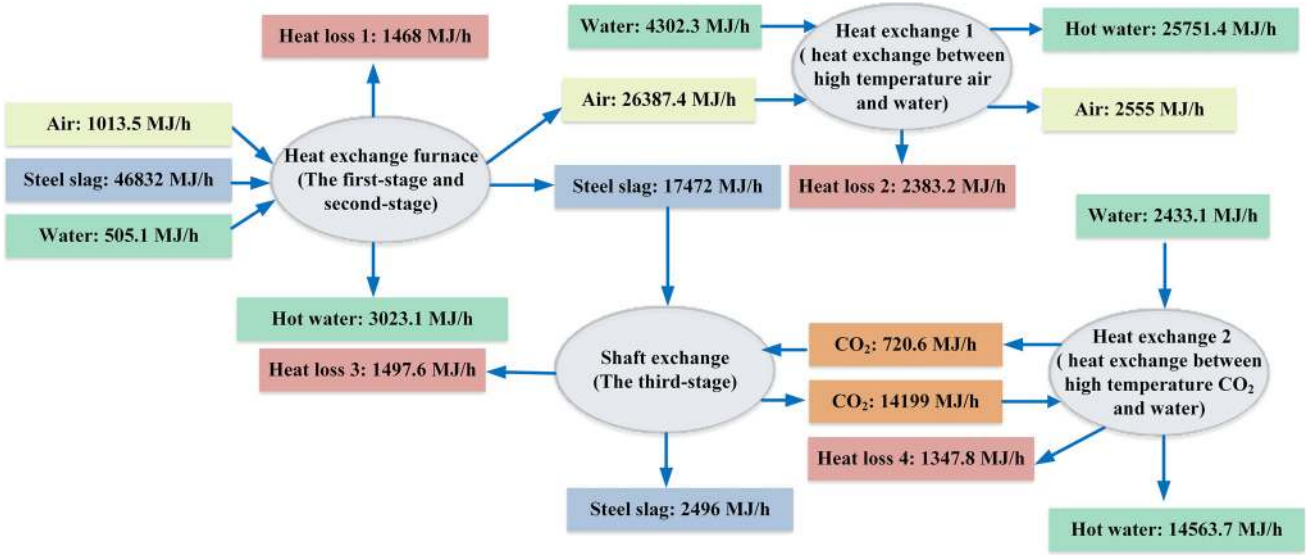

Fig. 6—The energy balance diagram of waste heat converted into usable heat energy.

data and previous research results[43,44] that the conversion rate of f-CaO in steel slag can be higher than 70 pct. Through the chemical reaction measurement ratio, each ton of steel slag can absorb about 240 mol of CO_2.

B. *Mass Balance and Energy Balance*

1. *Initial conditions and setting of parameters*

(1) The steel slag treatment plant is proposed to be located in an independent and closed field, and the steel slag is transported into the plant by special transport conveyance. In a steel plant that produces 1.5 million tons of steel each year, its steel slag output is about 10 pct of steel. So 150 thousand tons of steel slag will be produced every year, and 20 tons of high-temperature steel slag will be produced every hour, if calculated according to 310 working days per year. The slag's specific heat is 1.248 kJ/kg·K, and the solidification latent heat of slag is 210 kJ/kg.[49,50]

(2) In the process of mass balance and heat balance, the device is divided into four parts for calculation, which are: heat exchange furnace (the first and second stage of heat exchange), the heat exchanger 1 (heat exchange between high-temperature air and water), shaft furnace (the third stage of heat exchange), the heat exchanger 2 (heat exchange between high-temperature CO_2 and water).

(3) The calculation of heat balance and mass balance are inseparable. Set 273.15 K, 1 atm as the reference points of enthalpy. The working medium's specific

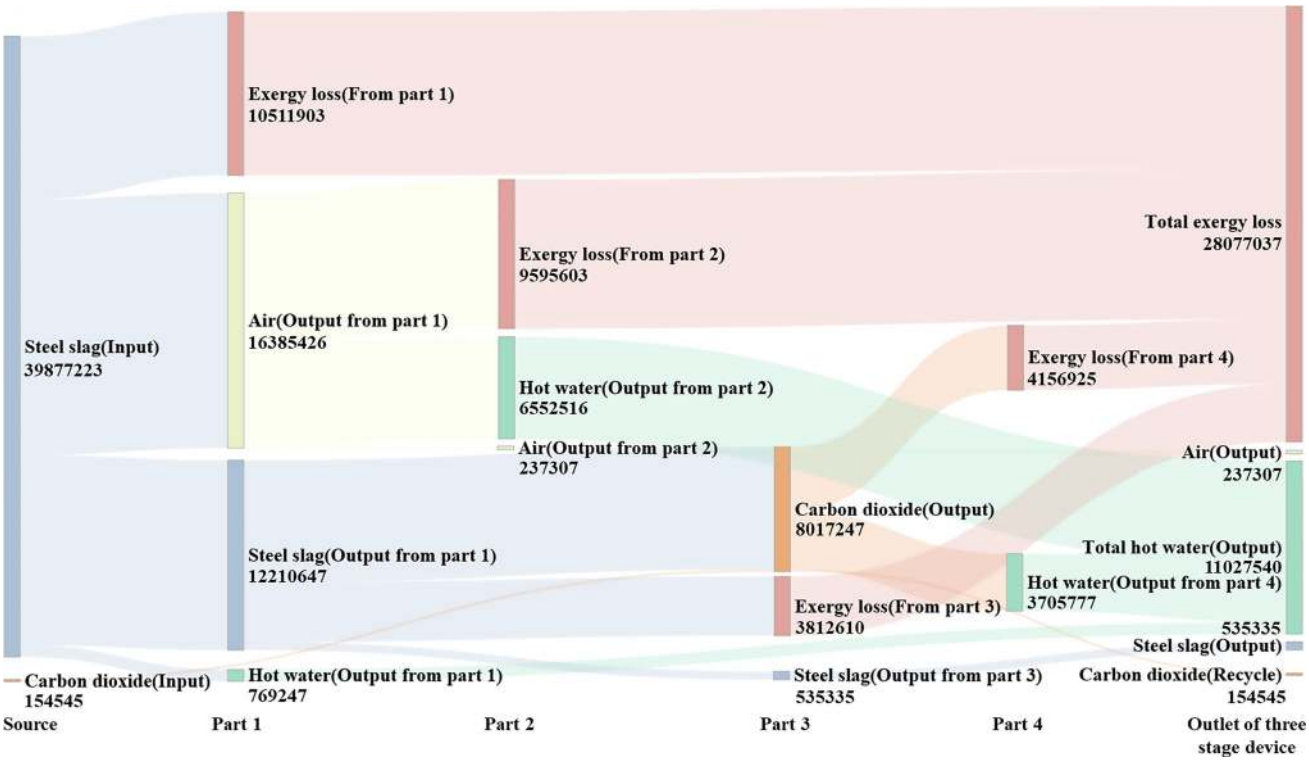

Fig. 7—The exergy diagram of waste heat converted into usable heat energy.

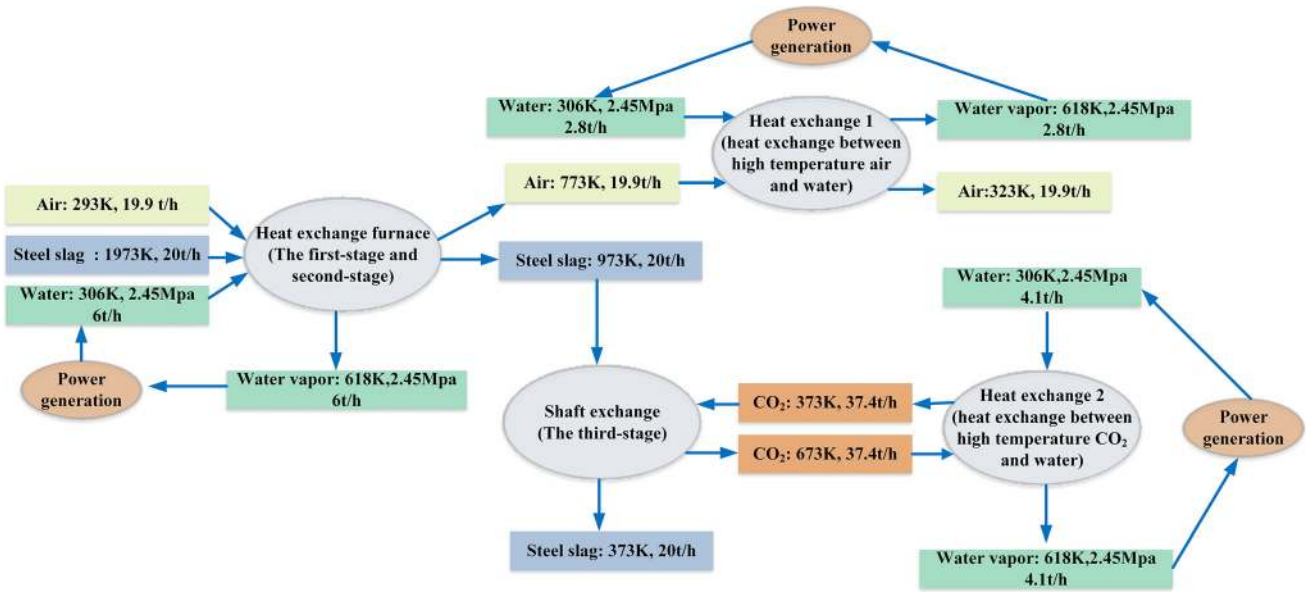

Fig. 8—The mass balance diagram of waste heat converted into electric energy.

enthalpy can be determined using the temperature and pressure of the active medium. Set the thermal efficiency of heat exchangers and the shaft furnace to 90 pct that of heat exchange furnace to 95 pct. At the inlet for working medium, the temperature is 293.15 K and the pressure is 1 atm. The mass flow of water in the first stage is 6000 kg/h.

The Q_{slag} is the heat provided by steel slag, and it can be calculated by the following formula.

$$Q_{\text{slag}} = C_p \times m_{\text{slag}} \times (T - T_{rt}) + r \times m_{\text{slag}} \qquad [1]$$

where C_p is the average specific heat of the slag, kJ/(kg·K);m_{slag} is the quantity of the slag per hour, kg/h;$T$is the input or output temperature, K;T_{rt} is

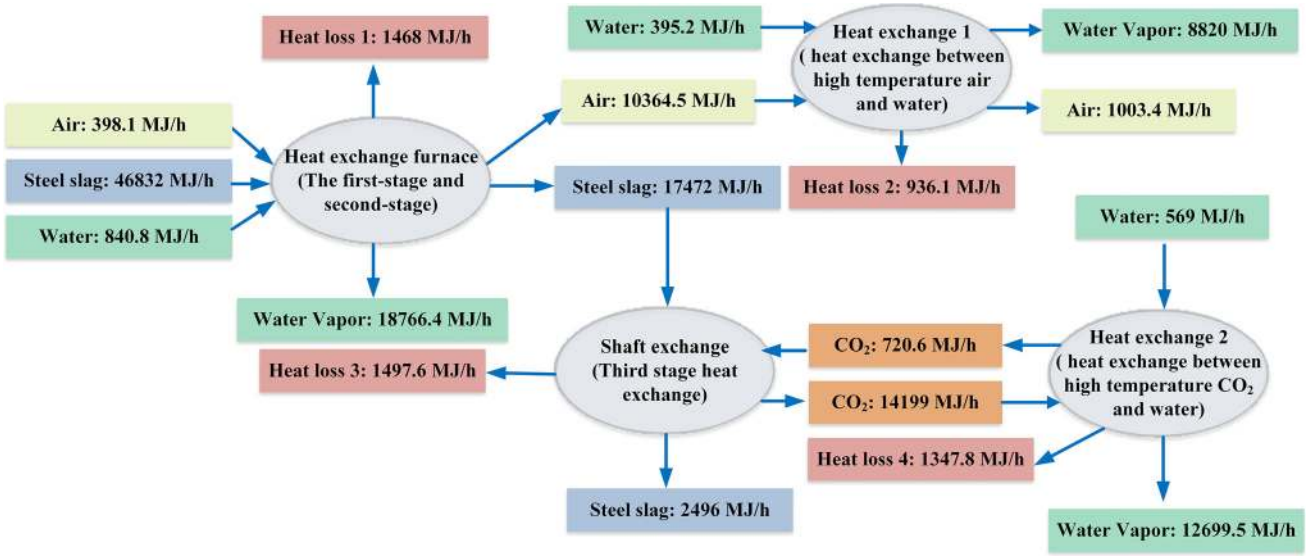

Fig. 9—The energy balance diagram of waste heat converted into electric energy.

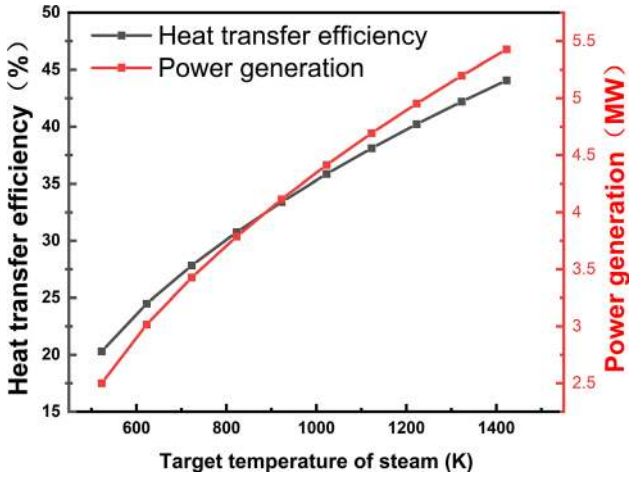

Fig. 10—The relationship between heat recovery rate and the temperature of the water vapor.

the reference temperature, K, which is equal to 273.15 K in this paper;r is the solidification latent heat, kJ/kg.

In this work, the working medium includes water, steam, air, and CO_2. The $Q_{\text{workingmedium}}$ is the heat provided by the working medium, and it can be calculated by the following formula.

$$Q_{\text{workingmedium}} = m_{\text{workingmedium}} \times h \quad [2]$$

where $m_{\text{workmedium}}$ is the mass flow of the working medium, kg/h;h is the specific enthalpy of the working medium under given input or output condition, kJ/kg.

According to the principle of balance between heat input and heat consumption, unknown working fluid flow can be calculated out through:

$$\sum Q_{\text{in}} = \sum Q_{\text{out}} \quad [3]$$

where $\sum Q_{\text{in}}$ represents all the heat input in each step, kJ/h. $\sum Q_{\text{out}}$ represents all the heat consumption in each step, kJ/h.

Thermal efficiency can be calculated by:

$$R = \frac{Q_{\text{total,vapor}}}{Q_{\text{total,slag}}} \quad [4]$$

where $Q_{total,slag}$ represents the exothermic heat of steel slag throughout the whole process, kJ/h. $Q_{total,vapor}$ represents the endothermic heat corresponding to the total amount of steam produced in the entire process, kJ/h.

(4) The heat exergy of the medium is calculated by the following formula:

$$E_{x,Q} = \left(1 - \frac{T_0}{T}\right) Q. \quad [5]$$

In this formula, $E_{x,Q}$is the heat of the medium, kJ/h; T is the temperature of the medium; T_0 is the ambient temperature, K, and Q is the heat carried by the medium, kJ/h.

The exergy utilization efficiency of each link can be calculated by the following formula:

$$\eta_{e_x} = \frac{\sum E_{x,Q\text{out}}}{\sum E_{x,Q\text{in}}}. \quad [6]$$

In the formula, η_{e_x} is the exergy efficiency; $\sum E_{x,\text{Qin}}$ is the total exergy input at the inlet, kJ/h; and $\sum E_{x,Q\text{out}}$ is the total exergy income at the outlet, kJ/h. Combining the results of heat balance and mass balance, the flow direction of exergy can be calculated. The detailed calculation process is described in the electronic supplementary material.

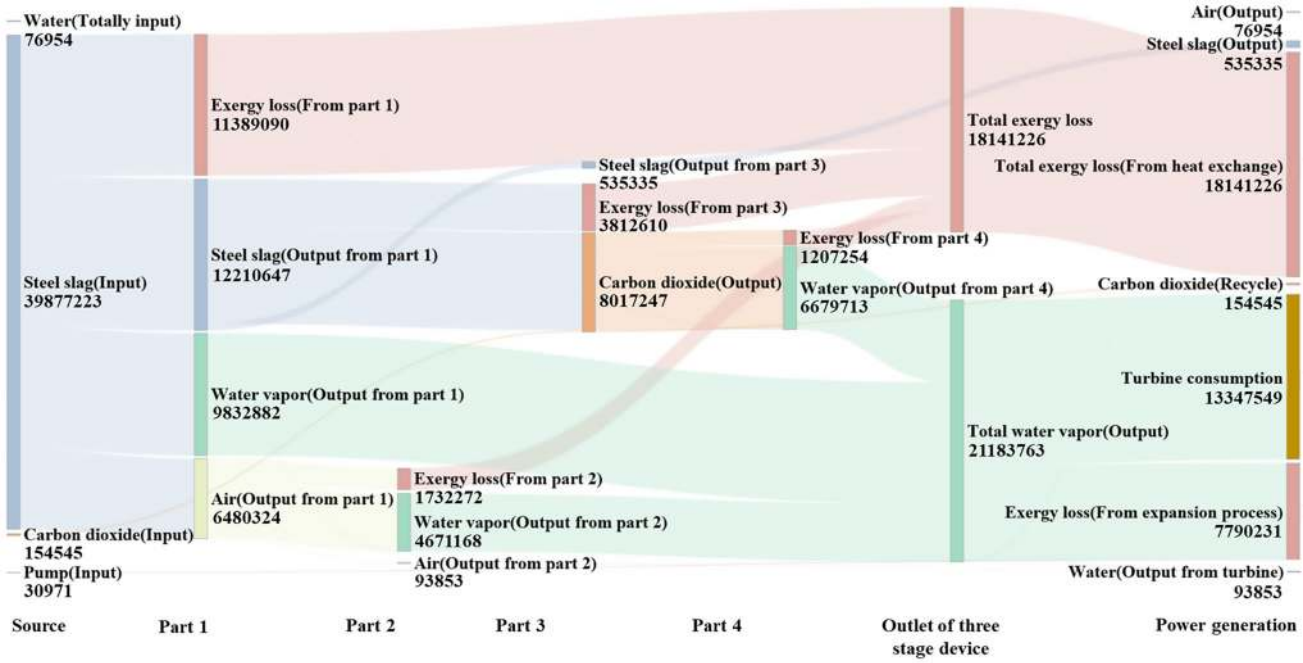

Fig. 11—The exergy diagram of waste heat converted into electric energy.

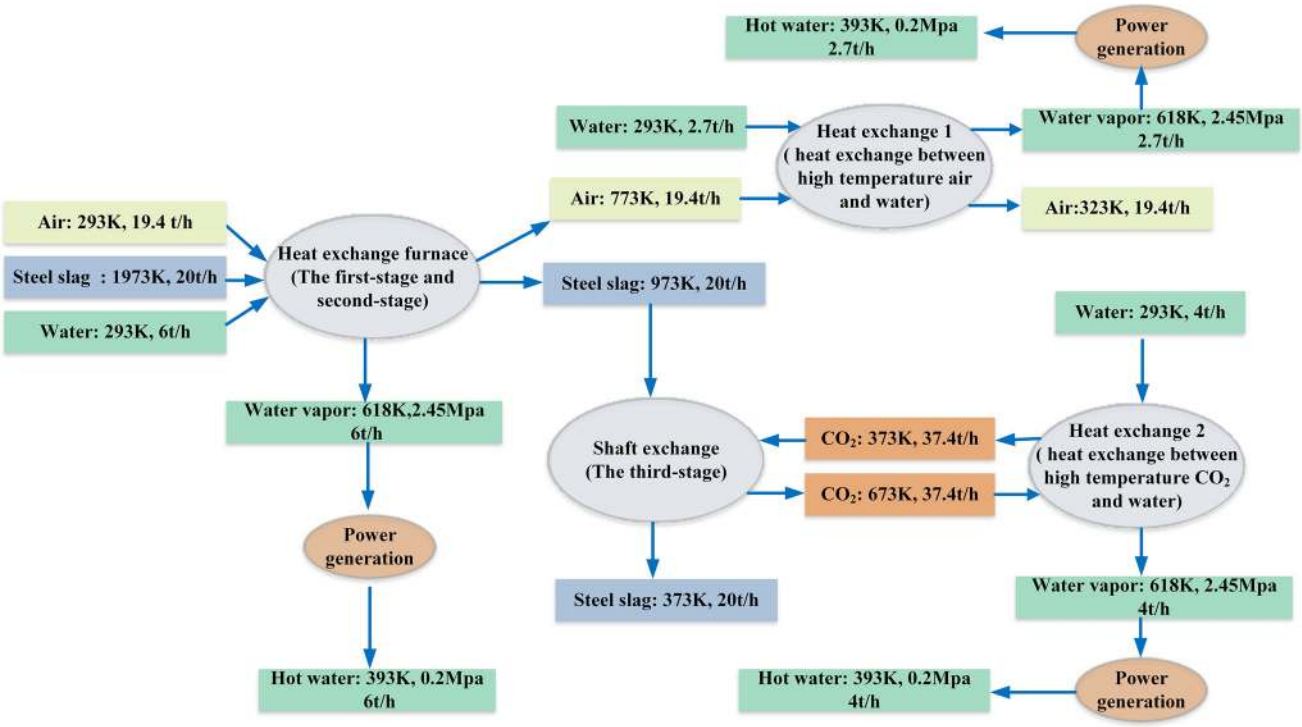

Fig. 12—The mass balance diagram of cogeneration of waste heat.

2. *Conversion of waste heat into usable heat energy*
When the waste heat is converted into usable heat energy, the results of mass balance and energy balance are shown in Figures 5 and 6. Calculated based on processing 20 t high-temperature steel slag per hour, the hot water at 393.5 K, 0.3 Mpa, which meets the water pressure requirement during delivery, can be produced at 86 t/h. The total heat recovery from the available hot water is 36097.7 MJ/h. Theoretically, the complete heat recovery in the slag is 44336 MJ/h. So the heat recovery rate R is:

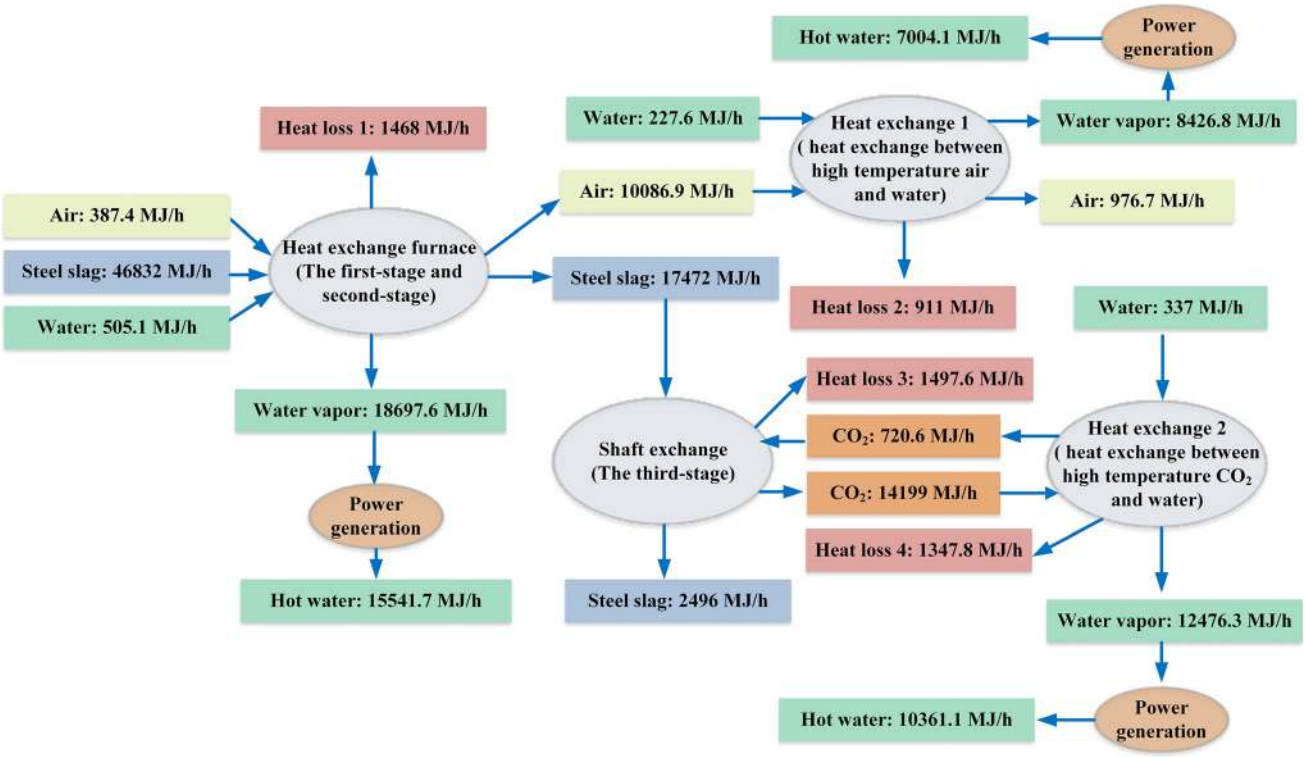

Fig. 13—The energy balance diagram of cogeneration of waste heat.

$$R = \frac{Q_{\text{total,vapor}}}{Q_{\text{total,slag}}} = 81.42\text{pct} \ . \qquad [7]$$

In the system that converts waste heat into usable heat energy, the exergy input is the heat exergy carried by the steel slag and CO_2 at the inlet as shown in Figure 7. In contrast, the exergy income is the heat exergy taken by the hot water at the outlet and the recycled CO_2. For heat exergy, the exergy efficiency of the overall system can be calculated by using the exergy value of each link in the figure as:

$$\eta_{e_x} = \frac{\sum E_{x,Q\text{out}}}{\sum E_{x,Q\text{in}}} = 27.93\,\text{pct}. \qquad [8]$$

3. *Conversion of waste heat into electricity*

The heat exchange process is included in the power generation cycle of waste heat. When the waste heat is converted into electricity energy, the results of mass balance and energy balance are shown in Figures 8 and 9. The isobaric heat absorption process is completely performed by the waste heat recovery device. In this paper, water vapor (618 K) is used as the intermediate heating medium. The generated steam is sent to the boiler, and the steam circulates between the devices in the Rankine cycle. The steam after the expansion process is returned to the three-stage device through the cooling tower and the pressurized water pump to realize circulation. Through heat balance and energy balance, the electricity generated by the recovered waste water vapor for work is 10859 MJ/h.

The heat recovery rate R is:

$$R = \frac{Q_{\text{total,vapor}}}{Q_{\text{total,slag}}} = 24.49\,\text{pct}. \qquad [9]$$

As the temperature of hot vapor for heat exchange changes, heat recovery rates and power generation vary. The specific relationship is shown in Figure 10.

The exergy diagram of waste heat converted into electric energy is shown in Figure 11. The exergy input is the heat exergy carried by the steel slag, CO_2, and water at the inlet, as well as that carried by the water pump. The exergy income is used by the steam turbine for power generation. The exergy of the whole system, the exergy of the heat carried by the recycled CO_2 and the super-cooled liquid water that is put into the heating process in the Rankine cycle, and the exergy efficiency of the overall system can be calculated by the exergy value of each link in the figure:

$$\eta_{e_x} = \frac{\sum E_{x,Q\text{out}}}{\sum E_{x,Q\text{in}}} = 33.83\,\text{pct} \qquad [10]$$

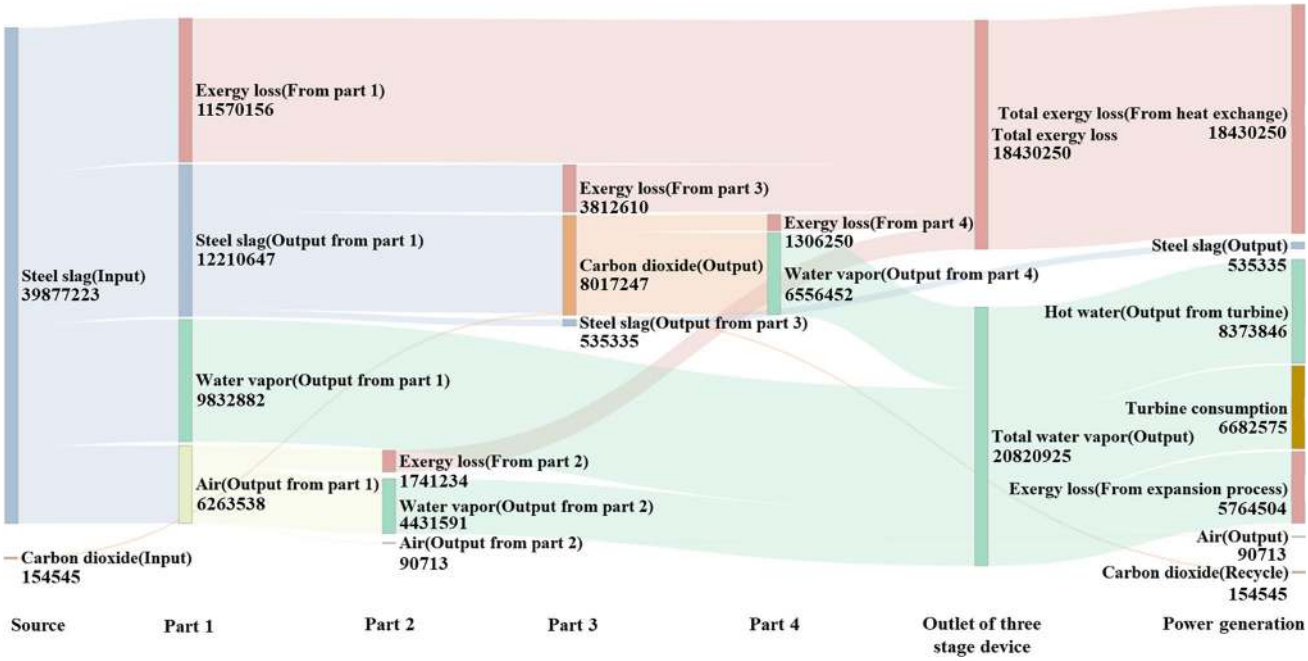

Fig. 14—The exergy diagram of cogeneration of waste heat.

4. *Cogeneration*
   When the waste heat is recovered through cogeneration, the results of mass balance and energy balance are shown in Figures 12 and 13. The high-temperature water vapor generated by heat exchange drives the steam turbine to generate power, and the water vapor after the work is used to produce hot water at 120 °C. The amount of electricity generated by work E is 5396.2 MJ/h (1.5 MW). The heat recovery rate R is :

$$R = \frac{Q_{\text{total,vapor}}}{Q_{\text{total,slag}}} = 83.98\,\text{pct}. \quad [11]$$

Figure 14 shows the exergy diagram of cogeneration of waste heat. In the cogeneration system, the exergy input is the heat exergy carried by the steel slag and CO_2 at the inlet, while the exergy income is the exergy used by the steam turbine for power generation, and that carried by the recycled CO_2. The heat exergy carried by the high-temperature water produced and the exergy efficiency of the overall system can be calculated by using the exergy value of each link in the figure:

$$\eta_{e_x} = \frac{\sum E_{x,Q\text{out}}}{\sum E_{x,Q\text{in}}} = 38\,\text{pct}. \quad [12]$$

From the perspective of exergy utilization, cogeneration is the most efficient method to recycle waste heat.

IV. CONCLUSION

This paper proposes a method for high-efficiency utilization of high-temperature molten steel slag with three stages and three media, introducing the technical route and equipment as well. The heat recovery efficiency and exergy efficiency are obtained through the calculation of mass balance and energy balance. From the perspective of energy recovery, the three-stage three-medium waste heat recovery process can recycle the heat of molten slag in the form of high-temperature steam and high-temperature air, and realize the cascade recovery of waste heat from steel slag. The heat recovery rate of steel slag is greater than 80 pct. From the perspective of resource recovery, this method fully utilizes the resource attributes of steel slag to produce low-temperature solid steel slag, which can be used as a raw material for new-type plates and floorings. From the ecological point of view, excessive CO_2 emission is the main cause of the greenhouse effect. This method can reduce coal burning through waste heat recovery and can absorb a large amount of CO_2 during the process. It also provides a new idea for making full use of the waste heat energy and the resource attributes of high-temperature molten steel slag.

ACKNOWLEDGMENTS

This research was funded by the National Key Research and Development Plan of China (2018YFC1901505 and 2018YFC1901503), National Natural Science Foundation of China (51672006), Shanxi Unveiling Bidding Project (20191101007), and the Ministry of Land and Resources Public Welfare Industry Research Project (201511062-02).

SUPPLEMENTARY INFORMATION

The online version of this article (https://doi.org/10.1007/s11663-021-02213-7).

REFERENCES

1. J.M. Allwood, J.M. Cullen, and R.L. Milford: *Environ. Sci. Technol.*, 2010, vol. 44, pp. 1888–94.
2. IEA, Iron and Steel Technology Roadmap. (IEA, Paris, 2020) https://www.iea.org/reports/iron-and-steel-technology-roadmap. Accessed 31 October 2021.
3. The world crude steel production data. https://www.worldsteel.org/. Accessed 15 March 2020.
4. Y.Q. Sun, Z.T. Zhang, L.L. Liu, and X.D. Wang: *Energies*, 2015, vol. 8, pp. 1917–35.
5. Z.W. Chen, H. Wang, Y.Q. Sun, L.L. Liu, and X.D. Wang: *Metall. Mater. Trans. B*, 2019, vol. 50, pp. 2930–41.
6. C.J. Shi: *J. Mater. Civil. Eng.*, 2004, vol. 16, pp. 230–36.
7. P. Bilski and J. Wojciechowski: *Arch. Metall. Mater.*, 2010, vol. 55, pp. 1137–45.
8. R. Zhang, Y. Wang, X. Zhao, J.X. Jia, C.J. Liu, and Y. Min: *Metall. Mater. Trans. B*, 2020, vol. 51, pp. 2021–29.
9. L. Řeháčková, S. Rosypalová, R. Dudek, J. Kukutschová, and J. Dobrovská: *Metalurgija*, 2015, vol. 54, pp. 455–58.
10. M.K. Oh, T.S. Kim, and J.H. Park: *Metall. Mater. Trans. B*, 2020, vol. 51, pp. 3028–38.
11. T.S. Jeong and J.H. Park: *Metall. Mater. Trans. B*, 2020, vol. 51, pp. 2309–20.
12. H.T. Shen and E. Forssberg: *Waste Manage.*, 2003, vol. 23, pp. 933–49.
13. S. Yüksel: *Environ. Dev. Sustain.*, 2018, vol. 19, pp. 1–16.
14. P.E. Tsakiridis, G.D. Papadimitriou, S. Tsivilis, and C. Koroneos: *J. Hazard. Mater.*, 2008, vol. 152, pp. 805–11.
15. J.W. Sun, Z.Q. Zhang, S.Y. Zhuang, and W. He: *Constr. Build. Mater.*, 2020, vol. 241, art. no. 118141.
16. W.G. Shen, M.K. Zhou, W. Ma, J.Q. Hu, and Z. Cai: *J. Hazard. Mater.*, 2009, vol. 164, pp. 99–104.
17. P. Suer, J.E. Lindqvist, M. Arm, and P. Frogner-Kockum: *Sci. Total Environ.*, 2009, vol. 407, pp. 5110–18.
18. P. Ahmedzade and B. Sengoz: *J. Hazard. Mater.*, 2009, vol. 165, pp. 300–305.
19. H. Kumar and S. Varma: *Int. J. Pavement Res. Technol*, 2021, vol. 14, pp. 232–42.
20. T. Gupta and S.N. Sachdeva: *Arab J Sci Eng*, 2020, vol. 45, pp. 8111–27.
21. R.I. Iacobescu, D. Koumpouri, Y. Pontikes, R. Saban, and G.N. Angelopoulos: *J. Hazard. Mater.*, 2011, vol. 196, pp. 287–94.
22. Y.H. Liao, G.X. Jiang, K.J. Wang, S. Qunaynah, and W.J. Yuan: *Constr. Build. Mater.*, 2020, vol. 265, p. 120301.
23. L.S. Li, M. Zhu, X. Li, Q. Wang, and R.J. Liu: *Key Eng. Mater.*, 2020, vol. 861, pp. 446–51.
24. J.L. Liao, Z.H. Zhang, J.T. Ju, and F.C. Zhao: *Adv. Mater. Res.*, 2013, vols. 834–836, pp. 378–84.
25. S. Imashuku, H. Tsuneda, and K. Wagatsuma: *Metall. Mater. Trans. B*, 2020, vol. 51, pp. 27–34.
26. X.K. Hou, D.L. Xu, B. Xue, and H.S. Li: *J. Build. Mater.*, 2012, vol. 15, pp. 588–95.
27. G. Wang, Y.H. Wang, and Z.L. Gao: *J. Hazard. Mater.*, 2010, vol. 184, pp. 555–60.
28. M. Gautier, J. Poirier, F. Bodénan, G. Franceschini, and E. Véron: *Int. J. Miner. Process*, 2013, vol. 123, pp. 94–101.
29. S.A. Mikhail and A.M. Turcotte: *Thermochim. Acta*, 1995, vol. 263, pp. 87–94.
30. C.W. Liu, S.G. Huang, P. Wollants, B. Blanpain, and M.X. Guo: *Metall. Mater. Trans. B*, 2017, vol. 48, pp. 1602–1612.
31. C. Liu, M. Guo, L. Pandelaers, B. Blanpain, and S. Huang: *Metall. Mater. Trans. B*, 2016, vol. 47, pp. 1–4.
32. F.C. Zhao, J.T. Ju, J.L. Liao, W.M. Kong, and Y.J. Dang: *Adv. Mater. Res.*, 2013, vols. 753–755, pp. 623–627.
33. X.S. Yang, Z.Q. Huo, Z. Zhang and Z.X. Yang, IOP Conference Series: Earth and Environmental Science, 2021, vol. 643, p. 012068 (7pp).
34. Y. Ye, S.P. Wu, C. Li, D. Kong, and B. Shu: *Materials*, 2019, vol. 12, p. 2322.
35. H. Tobo, Y. Ta, M. Kuwayama, Y. Hagio, K. Yabuta, H. Tozawa, T. Tanaka, K. Morita, H. Matsuura, and F. Tsukihashi: *ISIJ Int.*, 2015, vol. 55, pp. 894–903.
36. E. Cheremisina, J. Schenk, L. Nocke, A. Paul, and G. Wimmer: *Metall. Mater. Trans. B*, 2019, vol. 50, pp. 1269–76.
37. Y. Sakurai, X. Yang, Y. Hisaka, and F. Tsukihashi: *Metall. Mater. Trans. B*, 2020, vol. 51, pp. 1039–47.
38. Y.X. Dai, J. Li, C.B. Shi, and W. Yan: *Ironmak. Steelmak.*, 2020, vol. 5, pp. 1–10.
39. N.M. Dowell, P.S. Fennell, N. Shah, and G.C. Maitland: *Nat. Clim. Change*, 2017, vol. 7, pp. 243–49.
40. P. Markewitz, W. Kuckshinrichs, W. Leitner, J. Linssen, P. Zapp, R. Bongartz, A. Schreiber, and T.E. Mueller: *Energy Environ. Sci.*, 2012, vol. 5, pp. 7281–305.
41. J. Wouter, J. Huijgen, G.-J. Witkamp, N. Rob, and J. Comans: *Environ Sci Technol*, 2005, vol. 39, pp. 9676–82.
42. D. Bonenfant, L. Kharoune, S. Sauve, R. Hausler, P. Niquette, M. Mimeault, and M. Kharoune: *Ind. Eng. Chem. Res.*, 2008, vol. 47, pp. 7610–16.
43. E.E. Chang, C.H. Chen, Y.H. Chen, S.Y. Pan, and P.C. Chiang: *J. Hazard. Mater.*, 2011, vol. 186, pp. 558–64.
44. E.E. Chang, S.Y. Pan, Y.H. Chen, H.W. Chu, C.F. Wang, and P.C. Chiang: *J. Hazard. Mater.*, 2011, vol. 195, pp. 107–14.
45. S.Y. Pan, T.C. Chung, C.C. Ho, C.J. Hou, Y.H. Chen, and P.C. Chiang: *Sci. Rep. UK*, 2017, vol. 7, p. 17227.
46. J. Yu and K.B. Wang: *Energ Fuel*, 2011, vol. 25, pp. 5483–92.
47. Z. Ghouleh, I. Rodrick, L. Guthrie, and Y. Shao: *Constr. Build. Mater.*, 2015, vol. 99, pp. 175–183.
48. W.G. Shen, Y. Liu, M.M. Wu, D. Zhou, and X. Xiong: *J. Clean. Prod.*, 2020, vol. 256, p. 120244.
49. L.Z. Yang, T. Jiang, G.H. Li, and Y.F. Guo: *High. Temp. Mat. Pr-Isr.*, 2017, vol. 36, pp. 615–21.
50. Yoshiaki. Kashiwaya, Tomohiro. Akiyama, and Yutaro. In-Nami: *ISIJ Int.*, 2010, vol. 50, pp. 1259–64.